The Journal of Chemical Physics

Unraveling exciton processes in $Ir(ppy)_3$:CBP OLED films upon photoexcitation

Cite as: J. Chem. Phys. **154**, 164101 (2021); https://doi.org/10.1063/5.0044177
Submitted: 14 January 2021 . Accepted: 02 April 2021 . Published Online: 22 April 2021

Stephen Sanderson, George Vamvounis, Alan E. Mark, Paul L. Burn, Ronald D. White, and Bronson W. Philippa

The Journal of Chemical Physics ARTICLE scitation.org/journal/jcp

Unraveling exciton processes in $Ir(ppy)_3$:CBP OLED films upon photoexcitation

Cite as: J. Chem. Phys. 154, 164101 (2021); doi: 10.1063/5.0044177
Submitted: 14 January 2021 • Accepted: 2 April 2021 •
Published Online: 22 April 2021

Stephen Sanderson,[1] George Vamvounis,[1] Alan E. Mark,[2] Paul L. Burn,[3] Ronald D. White,[1] and Bronson W. Philippa[1,a)]

AFFILIATIONS

[1]College of Science and Engineering, James Cook University, Townsville, QLD 4811, Australia
[2]School of Chemistry and Molecular Biosciences, The University of Queensland, Brisbane, QLD 4072, Australia
[3]Centre for Organic Photonics & Electronics, School of Chemistry and Molecular Biosciences, The University of Queensland, Brisbane, QLD 4072, Australia

[a)]**Author to whom correspondence should be addressed:** bronson.philippa@jcu.edu.au

ABSTRACT

Emissive layers in phosphorescent organic light-emitting diodes commonly make use of guest–host blends such as $Ir(ppy)_3$:CBP to achieve high external quantum efficiencies. However, while the $Ir(ppy)_3$:CBP blend has been studied experimentally, crucial questions remain regarding how exciton diffusion is dependent on the distribution of the guest in the host, which can currently only be addressed at the atomic level via computational modeling. In this work, kinetic Monte Carlo simulations are utilized to gain insight into exciton diffusion in $Ir(ppy)_3$:CBP blend films. The effects of both guest concentration and exciton density on various system properties are analyzed, including the probability of singlet excitons being converted to triplets, and the probability of those triplets decaying radiatively. Significantly, these simulations suggest that triplet diffusion occurs almost exclusively via guest–guest Dexter transfer and that concentration quenching of triplets induced by guest–guest intermolecular dipole-dipole interactions has a negligible effect at high exciton densities due to the prevalence of triplet–triplet annihilation. Furthermore, results for vacuum deposited morphologies derived from molecular dynamics simulations are compared to the results obtained using a simple cubic lattice approximation with randomly distributed guest molecules. We show that while differences in host-based processes such as singlet diffusion are observed, overall, the results on the fate of the excitons are in good agreement for the two morphology types, particularly for guest-based processes at low guest concentrations where guest clustering is limited.

I. INTRODUCTION

Phosphorescent organic light-emitting diodes (OLEDs) are already used in commercial displays and offer the potential for high efficiency lighting with a theoretical maximum internal quantum efficiency of 100%.[1–4] In particular, guest–host OLEDs in which a host matrix is blended with a phosphorescent guest emitter are highly promising. Such devices achieve this high efficiency using emitters based on heavy metal atoms with strong spin–orbit coupling capable of promoting inter-system crossing (ISC) of excitons from the singlet to the triplet state, as well as radiative triplet emission.[2,5–7]

An archetypal phosphorescent OLED blend that has a reported high efficiency is composed of *fac*-tris(2-phenylpyridine)iridium(III) [$Ir(ppy)_3$] as the guest and 4,4′-bis(*N*-carbazolyl)biphenyl (CBP) as the host. This blend has been studied extensively to determine properties such as the optimal guest concentration,[8] exciton lifetimes and diffusion mechanisms,[9–14] and loss processes, such as triplet–triplet annihilation and non-radiative triplet decay.[15–18] $Ir(ppy)_3$:CBP blends have also been subject to detailed computational analysis, with molecular dynamics (MD) simulations showing that guest molecules tend to form clusters within the blend, rather than being randomly distributed,[19] and kinetic Monte Carlo (KMC) simulations revealing that charge diffusion is primarily guest-based, with guest clusters acting as multi-molecule traps.[20] However, questions remain regarding the details of the exciton diffusion process, particularly concerning the degree of triplet guest-confinement.

Here, we investigate exciton diffusion and exciton–exciton interactions in $Ir(ppy)_3$:CBP blend films using KMC techniques to simulate photoexcitation experiments. The efficiency of these simulations has enabled a wide parameter space to be sampled while maintaining good statistics. The sensitivity of the calculations to the details of the film morphology generation method was also investigated by comparing results of films at 6 wt. %[8] guest concentration obtained using a randomized cubic lattice structure, with those obtained using morphologies generated with MD simulations in which the process of vacuum deposition has been modeled explicitly in atomic detail.

II. METHODOLOGY

Exciton-only KMC simulations were performed with 12 different initial densities of randomly generated singlets between 3×10^{16} cm^{-3} and 3×10^{19} cm^{-3} to emulate short laser pulses of varying intensity and give realistic initial excitation densities.[21] The KMC model was based on the work we have published previously.[20,22] Singlet generation was treated as instantaneous at the beginning of the simulation. A uniform generation profile was used, meaning that all molecules in the system had an equal probability of singlet generation. If a chosen generation site was already occupied, that singlet was discarded and replaced. We note that only excitons and exciton–exciton (and not exciton–polaron) interactions were considered in this model to enable efficient simulations that do not require computationally expensive evaluation of electrostatic interactions, thereby allowing a wide parameter space to be sampled.

An overview of the modeled processes is provided in Fig. 1. Upon photoexcitation of the blend, singlets were allowed to diffuse via host–host and host–guest Förster transfer events.[12] Once a singlet was on a guest molecule, it could cross into the triplet state via ISC, and it was assumed based on the fast ISC rate of $Ir(ppy)_3$[15] that the singlet did not diffuse any further. That is, guest–guest and guest–host singlet transfers were not considered in the model. Competing with this singlet to triplet conversion process were radiative and non-radiative singlet decay events on the host. These decay processes were treated as having a fixed rate and were only considered for singlets on the host molecules (again due to the fast ISC rate once on the guest).

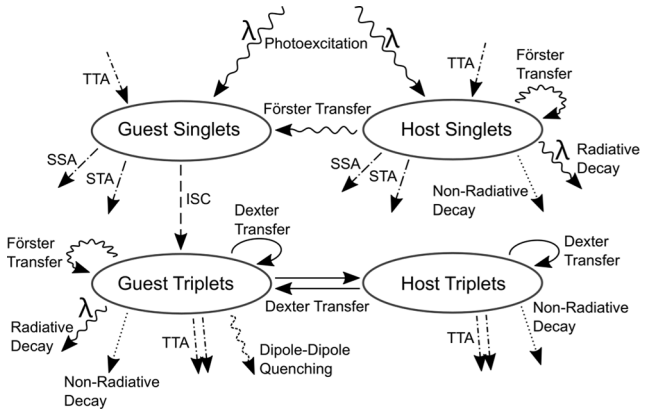

FIG. 1. Flowchart of the modeled processes and how they relate to the populations of singlets and triplets on guest and host molecules, where TTA is triplet–triplet annihilation, STA is singlet–triplet annihilation, SSA is singlet–singlet annihilation, and ISC is intersystem crossing.

Once a triplet formed on a guest, it was allowed to diffuse via both Dexter and Förster transfer events. Triplet Förster transfer events were considered for guest–guest transfers only, as Förster transfer from the guest to the host is unlikely given the relative triplet energies. In addition, the weak spin–orbit coupling of CBP[23] means that triplet formation on the host by ISC has a low probability. Triplet Dexter transfer events were allowed for guest–guest, guest–host, host–host, and host–guest transfers. The radiative and non-radiative triplet decay rates were fixed, with values dependent on the molecule type.

In addition, a triplet loss process with r^{-6} distance dependence that is independent of the triplet density has been observed when $Ir(ppy)_3$ molecules are in close proximity.[15,17,18,24] While the exact physical description of this process is unclear, it has previously been attributed to different factors including the formation of a weakly emissive excimer state,[15] repeated intermolecular energy transfer (emission and absorption between chromophore pairs) leading to the deactivation of the excited state,[17,24] and to excitation transfer to a quencher.[18] In this work, we model this triplet loss process as a dipole–dipole interaction[25] with a thermal activation energy of 170 meV. This value was chosen to fit the concentration dependent photoluminescence efficiency of $Ir(ppy)_3$:CBP blends, as presented by Kawamura *et al.*[26] (see Fig. S1 of the supplementary material), and is reasonably close to the value of 121 meV reported elsewhere.[16,17] The event rates for this process were parameterized in the same manner as guest–guest Förster transfer events [see Eq. (3) below] and were calculated for all neighboring guest molecules within a 5 nm radius. Triplets that undergo this transfer were removed from the system immediately for simplicity. To differentiate from other concentration quenching processes, we will refer to this process as dipole–dipole quenching. Note that while we calculated this dipole–dipole quenching rate in terms of activation energy, it could instead, without any significant change to the rate calculation, be interpreted as a probability that a given Förster transfer event results in the deactivation (loss) of that triplet. Note also that although the occupation state of the neighboring guest molecule was not considered in these rates for simplicity, this has no meaningful effect on the overall probability of radiative triplet decay, as both dipole–dipole quenching and triplet–triplet annihilation were assumed to result in the loss of one triplet.

To explore the effect of guest concentration, the simulations were repeated for all integer guest concentrations between 1 and 15 wt. %. The morphologies used for these simulations were based on a cubic lattice with randomly distributed emitter molecules. To validate the use of this cubic lattice approximation, the KMC simulations were also performed using the morphology of a blend containing 6 wt. % guest, generated by simulating the process of vacuum deposition using molecular dynamics techniques.[19,27,28]

To ensure sufficient statistical accuracy, the results for each concentration were averaged over five cubic lattice morphology realizations, with at least 20 repeats per realization per data point and up to 200 repeats at low initial excitation density. To obtain converged results at extremely low exciton densities where less than one singlet would be present in the periodic volume on average, simulations were performed in which excitons were treated as non-interacting.

In this case, 1000 singlets were generated, and 20 repeat simulations were used per morphology realization. Note that in the results, the lowest initial excitation density plotted corresponds to this non-interacting case. For the MD-generated morphologies, three realizations were used with at least 100 repeats per realization. For a clearer comparison between results from the MD-generated morphology and those from the cubic lattice morphology, up to 2000 repeats per realization were used at low exciton densities in the 6 wt. % guest blends.

A. Kinetic Monte Carlo simulations

The basic details of the KMC model used for these simulations have been described in our previous work.[20] Graphics Processing Unit (GPU) acceleration was used for efficient parallel rate computation and event selection, and random numbers were sampled using the permuted congruential generator (PCG) algorithm.[33]

To ensure that all exciton transfers with a reasonable probability were captured, Dexter transfer events were allowed for all neighbors with a center of mass (CoM) distance less than 3 nm, and Förster transfers were allowed within a radius of 5 nm. A Dexter or Förster transfer of a singlet or triplet to a destination site that was already occupied (regardless of whether that site was a guest or a host) resulted in an exciton–exciton interaction described by[14,34,35]

$$\begin{aligned} S_1 + S_1 &\rightarrow S_1 + S_0, \\ T_1 + S_1 &\rightarrow T_1 + S_0, \end{aligned} \tag{1}$$

or

$$T_1 + T_1 \rightarrow S_1 + S_0,$$

where S_1 is the first singlet excited state, T_1 is the first triplet excited state, and S_0 is the ground state. All triplet–triplet interactions were treated as resulting in a singlet for simplicity,[14,36] noting that this singlet will quickly cross back to the triplet state if it is on a guest molecule. To simplify the tracking of diffusion lengths and lifetimes, the quenched exciton was assumed to be the one undergoing the transfer, except in the case of singlet–triplet annihilation (STA) where the singlet was always quenched.

Dexter transfers were considered for triplet excitons only.[12,18] The rates were calculated using the Miller–Abrahams equation,[37–39]

$$\nu_{ij}^{(D)} = \nu_0 \exp(-2\gamma r_{ij}) \begin{cases} \exp\left(\frac{-\Delta E}{k_B T}\right), & \Delta E > 0 \\ 1, & \Delta E \leq 0, \end{cases} \tag{2}$$

where $\Delta E = E_j - E_i$ is the difference in energy between the destination site j and the source site i, γ is the inverse localization radius, r_{ij} is the distance between molecular centers of mass, ν_0 is the attempt-to-hop frequency, k_B is Boltzmann's constant, and T is the temperature. ν_0 for transfers between different molecular species was taken as the geometric mean, $\sqrt{\nu_0^{(i)}\nu_0^{(j)}}$, to allow potential guest–host and host–guest triplet Dexter transfers.[38,40] However, guest to host Dexter transfers are significantly less likely due to the 0.2 eV barrier presented by the difference in triplet energies.

Förster transfer event rates were calculated as[9,13,39,41–44]

$$\nu_{ij}^{(F)} = \frac{1}{\tau}\left(\frac{R_0}{r_{ij}}\right)^6 \begin{cases} \exp\left(\frac{-\Delta E}{k_B T}\right), & \Delta E > 0 \\ 1, & \Delta E \leq 0, \end{cases} \tag{3}$$

where τ is the exciton lifetime (such that $\tau^{-1} = \nu_{radiative} + \nu_{non\text{-}radiative}$) and R_0 is the Förster radius. The energetic disorder of the singlet and triplet states was assumed to be Gaussian in nature.[14,38,45]

A summary of the constants used in the KMC simulations is provided in Table I.

B. Morphology generation

1. Cubic lattice

Simulation boxes of 56 × 56 × 53 molecular sites on a cubic lattice were generated with a lattice spacing of 0.89 nm[20] so as to

TABLE I. Summary of simulation constants.

Parameter	Symbol	Value	References
Lattice spacing	a	0.89 nm	20
Temperature	T	300 K	
Inverse localization radius	γ	1.65 nm^{-1}	18 [a]
Förster radius	$R_0^{(S,host\text{-}host)}$	2.2 nm	12
	$R_0^{(S,host\text{-}guest)}$	2.8 nm	9
	$R_0^{(T,guest\text{-}guest)}$	2.1 nm	13
Dexter transfer prefactor	$\nu_0^{(T,host)}$	5.5×10^6 s^{-1}	[b]
	$\nu_0^{(T,guest)}$	1.08×10^{11} s^{-1}	18
Triplet decay rate	$\nu_{radiative}^{(T,guest)}$	7.5×10^5 s^{-1}	11 and 28
	$\nu_{non\text{-}radiative}^{(T,guest)}$	2.3×10^4 s^{-1}	11
	$\nu_{non\text{-}radiative}^{(T,host)}$	71.43 s^{-1}	14
Singlet decay rate	$\nu_{radiative}^{(S,host)}$	1.2×10^9 s^{-1}	9 and 10
	$\nu_{non\text{-}radiative}^{(S,host)}$	8×10^8 s^{-1}	9 and 10
Inter-system crossing rate	$\nu_{ISC}^{(guest)}$	1×10^{13} s^{-1}	15
Triplet energy	$E_T^{(host)}$	2.6 eV	29–31
	$E_T^{(guest)}$	2.4 eV	30
Singlet energy	$E_S^{(host)}$	3.1 eV	[c]
	$E_S^{(guest)}$	2.6 eV	[d]
Energetic disorder of exciton states	σ	30 meV	14 [e]

[a] For simplicity, the inverse localization radius for triplet excitons in CBP was assumed to be equal to that of $Ir(ppy)_3$.
[b] Triplet Dexter transfer rates in CBP were chosen such that the average triplet diffusion length was 140 nm[14] in a neat, fully periodic, cubic lattice system.
[c] The singlet energy of CBP was approximated as the HOMO–LUMO gap.
[d] The S_1 energy of $Ir(ppy)_3$ has been calculated to be 0.2 eV above the T_1 energy.[32]
[e] Energetic disorder was assumed to be the same throughout the system for both singlets and triplets.

represent a ~47 nm thick active layer with 50 nm periodic directions. Guest molecules were assigned randomly, with a probability based on the desired molecular concentration. The system was periodic in the x–y plane, with open boundaries in the z direction.

2. Vacuum deposition

To generate a more physically realistic morphology for a 6 wt. % guest concentration, MD simulations of the vacuum deposition process were performed using the method described previously.[19,27,28] Briefly, beginning with a graphene substrate, guest and host molecules were randomly chosen with random orientations and inserted ~3 nm above the top of the film at random positions, ensuring that simultaneously inserted molecules were separated by at least 2 nm. Each atom of these molecules was assigned a random velocity sampled from a Boltzmann distribution so that the overall molecule would have a random angular momentum. The sign of the vertical component of each initial velocity was set such that the molecule would move toward the substrate. The system was then allowed to evolve in time until the molecules reached the surface of the film, the point at which the insertion process was repeated until the desired film size was reached. The films were then allowed to equilibrate for 10 ns and were analyzed without a further annealing step.

The dimensions of the periodic simulation box in the x and y dimensions were 17.04 and 16.72 nm, respectively. CBP and $Ir(ppy)_3$ molecules were selected randomly in the appropriate ratio and were deposited eight at a time at 16 ps intervals onto a graphene substrate. The atoms in the substrate were assigned atom type "C" in the GROMOS 54A7 forcefield[46] and were harmonically restrained (k_H = 2 × 10^4 kJ mol^{-1} nm^{-2}). The interaction parameters for $Ir(ppy)_3$ were identical to those used by Tonnelé *et al.*[19] and Gao *et al.*[28] The interactions for CBP were assigned using the Automated Topology Builder (ATB) version 1.0.[47]

The simulations were performed using GROMACS 2018.3 with GPU acceleration,[48] with a time step of 2 fs. The temperature was controlled at 300 K using a Berendsen thermostat with a 0.1 ps coupling time.[19,49] The pair list for non-bonded interactions was updated every 20 fs with a cutoff radius of 1.4 nm. Electrostatic interactions were truncated beyond a cutoff of 1.4 nm using a reaction field correction with a relative permittivity of 10.[19,50] Bond lengths were constrained to their equilibrium values using the Linear Constraint Solver (LINCS) algorithm.[51] To reduce high frequency oscillations and improve integration, the mass of the hydrogen atoms was increased by 3 amu, which was correspondingly subtracted from their bonded neighbors to maintain the correct molecular mass. Despite this, using an order parameter of 4 and 1 iteration for LINCS resulted in the development of a velocity gradient beyond 1500 deposition steps (12 000 molecules). This was suppressed by increasing the number of iterations in LINCS to 2 after that point. A total of 20 000 molecules were deposited for a layer height of ~48 nm. The final layer was then replicated in the periodic directions for a total size of ~51 × 51 × 48 nm^3 (180 000 molecules).

III. RESULTS

A. Cubic lattice

To gain a full picture of exciton behavior upon photoexcitation, we begin by analyzing the fate of singlet excitons that formed on the host molecules. Figure 2 shows the percentage of singlets that are able to transfer to a guest molecule and undergo intersystem crossing as a function of the initial density of singlets and the wt. % concentration of the guest. This indicates that at low exciton densities, the proportion of singlets generated in the host that are able to transfer to a guest molecule and cross into the triplet state is relatively insensitive to the guest concentration above ~3 wt. %. Note that the reduction in triplet formation on the guest at higher initial excitation densities is almost entirely due to singlet–singlet annihilation on the host, which quenches as much as 55% of singlets at a low guest concentration. Singlet decay accounts for the remainder of the loss and is relatively insensitive to the initial excitation density below 1 × 10^{18} cm^{-3}. A maximum value of ~5% singlet loss due to singlet decay was observed at a guest concentration of 1 wt. %, and the

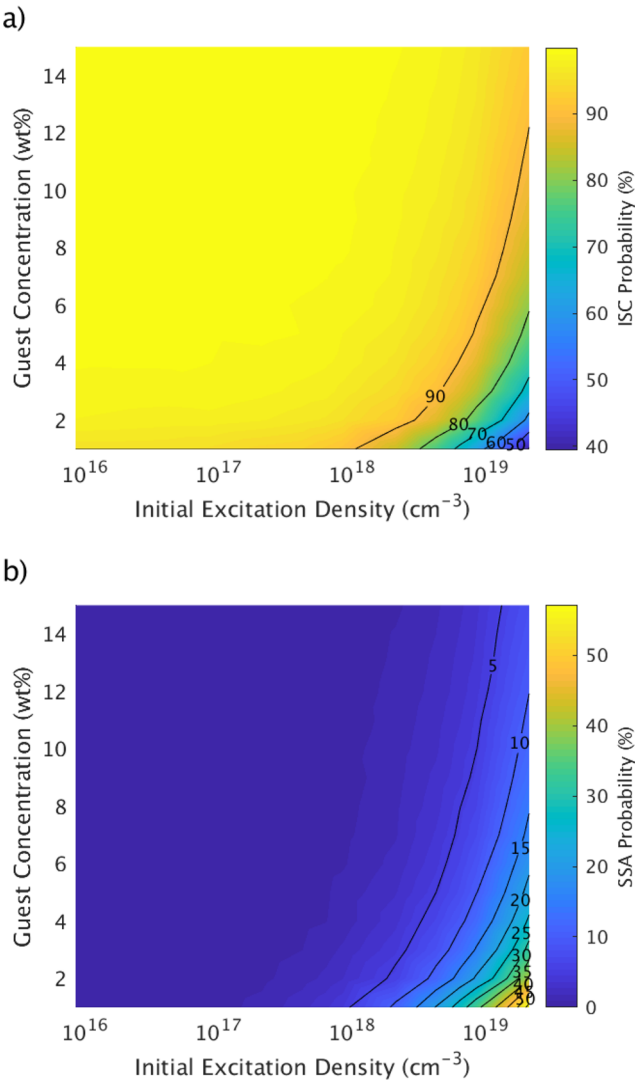

FIG. 2. Probability that a singlet formed on a host molecule (a) reaches a guest molecule and undergoes inter-system crossing or (b) is quenched by singlet–singlet annihilation (SSA).

singlet decay probability was less sensitive to excitation density at higher guest concentrations where the process of a singlet transferring to the guest and crossing to the triplet state is faster. A plot of the probability of radiative and non-radiative singlet decay is provided as Fig. S2 of the supplementary material. Singlet–triplet quenching was extremely rare in these systems and did not result in significant singlet loss.

It is also evident from Fig. 2 that the onset of singlet–singlet annihilation on the host is dependent on the guest concentration. Higher guest concentrations allowed shorter diffusion distances to guest molecules, thereby reducing the likelihood of singlet–singlet interactions or singlet decay. Considering that charge transport has been shown to occur predominantly on or near the guest, with >75% of excitons forming within 2 nm of a guest molecule even at 2 wt. % guest concentration,[20] the singlet diffusion length would be shorter than observed in these simulations where singlets were randomly generated, thus further reducing the probability that a singlet is lost through either singlet–singlet annihilation or radiative/non-radiative decay. Note that we define the diffusion length as the length of the displacement vector of the exciton undertaking a random walk, equal to the vector sum of its hops.

Once a triplet exciton is formed on the guest, it is able to diffuse via Dexter exchange, as well as guest–guest Förster transfer. As expected, due to the long triplet lifetime and low emission/absorption overlap of $Ir(ppy)_3$, it was found that triplet diffusion occurs predominantly via Dexter transfer, typically making up >97% of triplet transfer events. In addition, as shown in Fig. 3, which shows the average number of unique molecules visited by a triplet as a function of guest concentration for various initial excitation densities, triplet diffusion occurs almost exclusively on the guest even at a low guest concentration, with the average guest–guest transfer distance increasing from ~1.3 nm at 15 wt. % to ~2 nm at 1 wt. %. This is an expected outcome given that the triplet energy of the host is around 0.2 eV higher than that of the guest. Note that the reduction in the number of molecules visited as the exciton density increases is primarily due to the increased triplet–triplet annihilation (TTA).

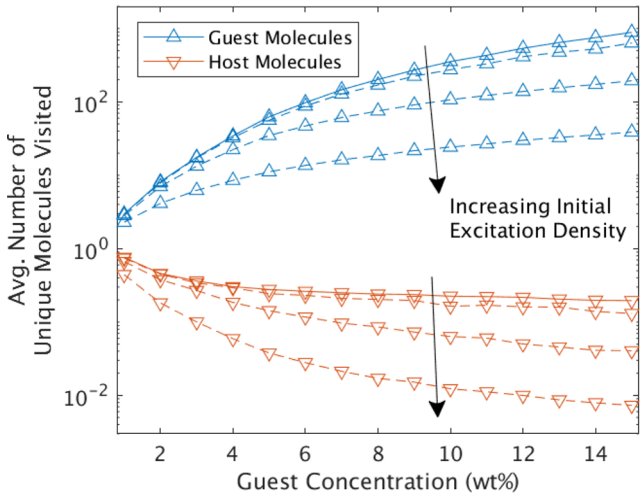

FIG. 3. Average number of unique guest and host molecules visited per triplet. Solid lines represent the non-interacting case, and dashed lines represent initial excitation densities of 1.1×10^{17} cm^{-3}, 1.1×10^{18} cm^{-3}, and 1.1×10^{19} cm^{-3}. Note the logarithmic scale on the y axis, as guest to host triplet transfer is an unlikely process.

The observed guest-based triplet diffusion leads to TTA being the primary loss process for triplets in these exciton-only systems at higher exciton densities. This is illustrated in Fig. 4, which shows the probabilities of radiative triplet decay and triplet loss due to TTA as a function of the initial excitation density and the concentration of the guest. Note that since TTA always results in the loss of one triplet and the conversion of the other one into a singlet in this model, it accounts for almost all triplet loss at a high exciton density. The resultant singlets formed on the guest are able to quickly cross back into the triplet state and are again subject to similar loss process statistics. Given the 10^2 difference in the average number of guest vs host molecules visited by a triplet evident in Fig. 3, the probability of TTA occurring on the host is highly unlikely.

The other main triplet loss processes considered were non-radiative decay and dipole–dipole quenching. The relative dependence of non-radiative decay on guest concentration and exciton density was identical to that of radiative decay [as shown in Fig. 4(a)]. The probability of a triplet being lost to dipole–dipole quenching is shown in Fig. 5, where it can be seen that while triplet loss via this process has a significant dependence on guest concentration at low exciton densities, it is largely independent of the guest concentration at higher exciton densities. This is because under high exciton density, the increase in TTA leads to a significant portion of triplets being lost on a time scale shorter than their natural decay time, thus suppressing the dipole–dipole quenching process. That is, at higher excitation densities, TTA is the dominant process for loss of the triplets.

B. Effect of morphology

A key question also addressed in this work was the extent to which differences in the morphology might affect the outcome of the KMC exciton simulations, specifically, whether the results obtained based on the commonly used practice of generating morphologies based on randomly assigning guest and host molecules to nodes on a cubic grid differ from those obtained using morphologies generated by simulating the process of vacuum deposition in atomic detail. The latter morphologies in which the guest is not randomly distributed have been extensively validated for the system in question, having been used to successfully predict a range of guest concentration dependent properties.[19,27] In this work, we only considered a guest concentration of 6 wt. % as this is the concentration that gives rise to the most efficient devices.[8] The main difference between the results obtained from the KMC simulations using the MD-based morphologies and those using morphologies based on a cubic lattice was that singlet excitons in the MD morphology were able to reach a guest molecule faster than in the cubic lattice morphology, as illustrated in Fig. 6. This difference is explained by the molecular packing in the MD system.

Increased guest clustering in the MD morphology results in a slightly larger mean CoM to CoM distance from a CBP molecule to the nearest $Ir(ppy)_3$ molecule (1.42 nm compared to 1.24 nm in the cubic lattice systems). However, the minimum value of this measurement was 0.45 nm in the MD system since CBP molecules are able to pack closely with the emitter, which is approximately half

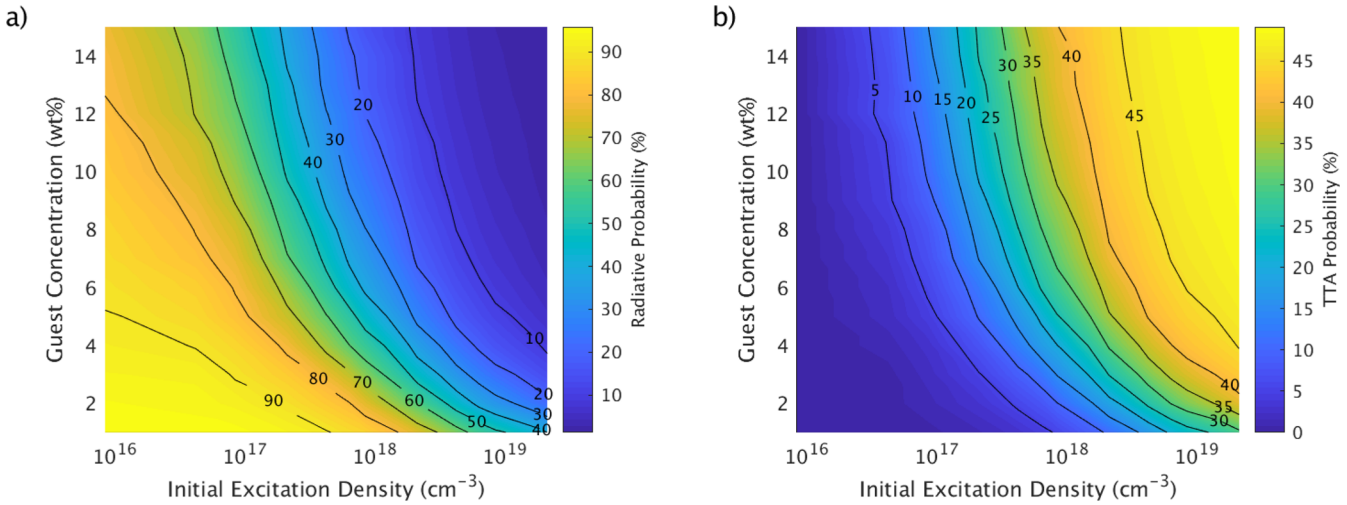

FIG. 4. (a) Probability that a triplet on a guest molecule decays radiatively. (b) Probability that a triplet is quenched via triplet–triplet annihilation. Note that, for every triplet quenched by TTA, another one is converted to a singlet, which is able to quickly cross back to the triplet state and is subject to similar fate statistics.

the minimum distance possible with a cubic lattice spacing of 0.89 nm (as required to give the correct molecular density). Thus, a singlet on a CBP molecule neighboring an Ir(ppy)$_3$ molecule is more likely to transfer to that guest molecule in the MD system than in the cubic lattice system. This leads to fewer instances of singlets hopping away from a neighboring guest, therefore slightly reducing the average time taken for a singlet to reach the guest, as well as the average singlet diffusion length.

In addition, spatial disorder within the host present in the MD-based morphology means there are, in effect, clusters of closely packed CBP molecules. Förster transfer of singlets between these closely packed CBP molecules is relatively fast, meaning a singlet may visit more unique CBP molecules before decaying, even though the diffusion length is slightly reduced. A comparison between the MD-based and cubic lattice morphologies of the singlet diffusion length and the number of unique host molecules visited in a 6 wt. % blend is provided as Fig. S3 of the supplementary material. It is important to note that the singlet diffusion length in either system is still significantly shorter than that of neat CBP and that for both of the morphologies examined, plots of the singlet diffusion length and the number of unique host molecules visited as a function of initial excitation density have the same qualitative shape.

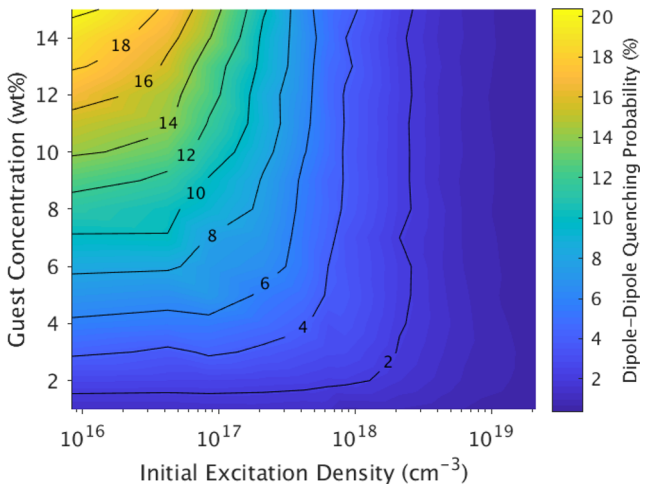

FIG. 5. Probability that a triplet is lost to dipole–dipole quenching.

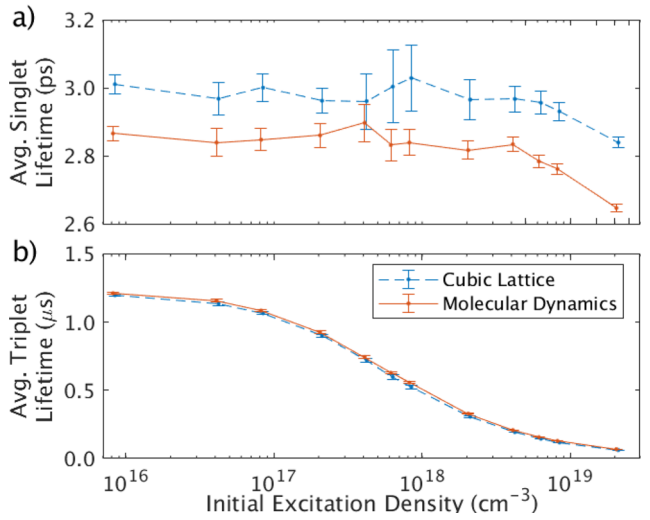

FIG. 6. Comparison of the mean (a) singlet and (b) triplet lifetimes between cubic lattice and MD-based systems at a 6 wt. % guest concentration. Error bars represent the standard deviation of the mean.

Interestingly, despite the observed differences and the potential limitations of the cubic lattice model, the proportion of singlet and triplet loss processes as a function of initial excitation density was essentially identical (within uncertainty) when the guest was at a concentration of 6 wt. %, regardless of whether the cubic lattice or MD-based morphology was used. This is illustrated in Fig. 7, which shows the probabilities of singlet ISC and radiative triplet decay. The exception to this was triplets at low initial excitation densities, where dipole–dipole quenching was slightly more prevalent in the cubic lattice system than in the MD-based system (see Fig. S4 of the supplementary material).

Importantly, triplet lifetimes were also nearly identical (Fig. 6), and only minor differences were observed in the triplet diffusion length and the number of unique guest and host molecules visited per triplet (plots of these quantities are provided as Figs. S5–S7 of the supplementary material). This suggests that within the limits of the theoretical approximations commonly employed in KMC transport modeling, results using a cubic lattice model can capture the key features of triplet dynamics in real systems, at least at low guest concentrations where the extent of guest aggregation is limited.

This result is further supported by an analysis of the guest–guest radial distribution function. Figure 8 shows the integral of the guest–guest (CoM to CoM) radial distribution function for the 6 wt. % cubic lattice and MD-based morphologies. The radial distribution functions themselves are provided in Fig. S8 of the supplementary material. From Fig. 8, it can be seen that the average concentration of guest molecules within a given radius around a chosen guest molecule is similar in both morphology cases. While the shape of the radial distribution function integral at $\sim r = 1$ nm for the MD-based morphology indicates some clustering of the guest, it is apparent that the step-wise nature of the cubic lattice approximates the underlying form. Figure 8 also offers an explanation toward why slightly more triplet loss due to dipole–dipole quenching was observed in the cubic lattice system compared to the MD-based system. It shows that despite the presence of guest clustering in the MD-based system, the lattice spacing results in a higher fraction of adjacent guest molecules <1 nm apart, thus increasing the probability of dipole–dipole quenching.

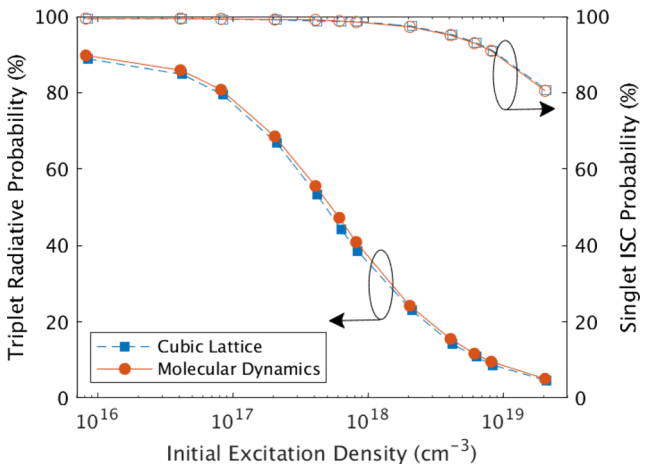

FIG. 7. Probability that a singlet formed in the host crosses to the triplet state on a guest (open symbols) and that the resultant triplet is able to radiatively decay (filled symbols) compared between the cubic lattice and MD-based systems at 6 wt. % guest concentration. Error bars representing the standard deviation of the mean are smaller than the marker size and are therefore omitted here. Plots comparing all triplet loss processes are provided as Fig. S4 of the supplementary material. Arrows indicate the relevant y axis.

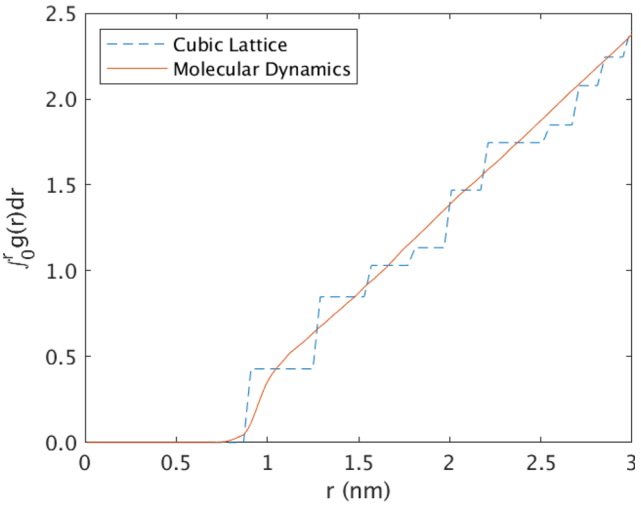

FIG. 8. Integral of the guest–guest (CoM to CoM) radial distribution function for cubic lattice and MD-based morphologies with a 6 wt. % guest concentration. The integral was used for clearer comparison due to the step-wise nature of the cubic lattice radial distribution function. The radial distribution functions themselves are provided in Fig. S8 of the supplementary material.

To confirm that this result was not simply a coincidence of the guest concentration tested, further MD morphologies were generated at 10 and 15 wt. % guest concentrations with a film thickness of ~20 nm using the same vacuum deposition protocol as the 6 wt. % systems. The guest–guest radial distribution functions of these films were compared to cubic lattice films with the same guest concentration and film thickness, and the results were found to be almost identical to the 6 wt. % case. These results are provided in Figs. S9 and S10 of the supplementary material. The observed comparable distributions of guest molecules at these higher guest concentrations indicate that those distributions determined from MD simulations are also well-approximated by a cubic lattice. As such, it would not be unreasonable to expect similar agreement between guest-based processes at other guest concentrations, at least under the approximations used in the current model in which molecular orientation is not considered. Similar differences in host-based processes are also expected although the magnitude of these differences may be less meaningful at higher guest concentrations where singlet diffusion lengths are shorter, and fewer host molecules are visited by a given singlet.

That comparable results for guest-based processes are found for this system where some limited clustering of the guest is present means that the lattice approach should also be applicable to similar systems where transport is dominated by hops between low-concentration trapping sites. The results could likely be further improved by introducing a random perturbation to the lattice sites

in order to smooth out the step-wise character shown in Fig. 8. We note that the exciton transport model presented here does not currently consider molecular orientation. However, this is a reasonable assumption as it has previously been shown that for $Ir(ppy)_3$:CBP blends, the $Ir(ppy)_3$ molecules tend to be randomly oriented in the bulk.[19] In that report, it was also found that the CBP molecules did not show a preferred orientation apart from molecules near the substrate (1–2 nm), which tended to preferentially align with the substrate. In our current work, we did not include a thermal anneal of the as-deposited films, and while we also observed random orientation of the $Ir(ppy)_3$ molecules, we observed a small bias for the CBP molecules to have their long axis align with the substrate in the bulk (see Fig. S11 of the supplementary material). That being said, in cases where there is a strong orientational order of components in the bulk and/or non-isotropic emission, it would be important for the orientation of the molecules within the film to be considered.

IV. SUMMARY

Kinetic Monte Carlo modeling was used to simulate exciton dynamics in $Ir(ppy)_3$:CBP OLED films under photoexcitation at a range of guest concentrations and exciton densities. It was found that even at low guest concentrations, triplet diffusion occurs almost exclusively via guest–guest Dexter transfers, thereby increasing the likelihood of triplet–triplet annihilation. This would imply that under normal device operation, triplet–polaron quenching will have a similarly large contribution to efficiency roll-off, as we have previously shown that charge transport is also predominantly guest-based.[20]

In addition, results from morphologies generated using molecular dynamics to simulate the process of vacuum deposition in atomic detail suggest that to a first approximation, KMC simulations based on a simple lattice model are representative of real systems in the case of processes that occur primarily on low concentration trapping sites. Thus, this method offers a relatively computationally efficient approach for modeling guest-dominated processes in guest–host phosphorescent OLEDs where the guest molecules are at low concentration and function as traps. However, while the fate of singlets in the modeled 6 wt. % guest blends was comparable between the cubic lattice and molecular dynamics morphologies, some differences were observed in their diffusion dynamics, indicating that processes involving the host molecules are not as well-captured in the cubic lattice model. We also note that further differences in both host- and guest-based processes may be observable under a more detailed model that explicitly accounts for factors such as molecular orientation.

SUPPLEMENTARY MATERIAL

See the supplementary material for additional supporting figures, as indicated in the text.

ACKNOWLEDGMENTS

We thank Dr. Thomas Lee, Dr. Martin Stroet, and Audrey Sanzogni for their assistance in configuring the molecular dynamics simulations and Dr. Paul Shaw for his insightful comments on exciton processes. We also acknowledge the computational resources provided by the James Cook University High Performance Computing facilities and the University of Queensland's Wiener cluster. S.S. was supported by an Australian Government Research Training Program Scholarship. P.L.B. is an Australian Research Council (ARC) Laureate Fellow (Grant No. FL160100067). This work was supported, in part, by the ARC Grant (No. DP180101421).

DATA AVAILABILITY

The data that support the findings of this study are available from the corresponding author upon reasonable request.

REFERENCES

[1] K. H. Kim and J. J. Kim, Adv. Mater. **30**, 1 (2018).
[2] H.-T. Mao, G.-F. Li, G.-G. Shan, X.-L. Wang, and Z.-M. Su, Coord. Chem. Rev. **413**, 213283 (2020).
[3] C. Adachi, M. A. Baldo, M. E. Thompson, and S. R. Forrest, J. Appl. Phys. **90**, 5048 (2001).
[4] M. A. Baldo, S. Lamansky, P. E. Burrows, M. E. Thompson, and S. R. Forrest, Appl. Phys. Lett. **75**, 4 (1999).
[5] B. Geffroy, P. le Roy, and C. Prat, Polym. Int. **55**, 572 (2006).
[6] K. Masui, H. Nakanotani, and C. Adachi, Org. Electron. **14**, 2721 (2013).
[7] N. Matsusue, Y. Suzuki, and H. Naito, Jpn. J. Appl. Phys., Part 1 **44**, 3691 (2005).
[8] S. Tokito and I. Tanaka, Electrochemistry **76**, 24 (2008).
[9] A. Ruseckas, J. C. Ribierre, P. E. Shaw, S. V. Staton, P. L. Burn, and I. D. Samuel, Appl. Phys. Lett. **95**, 2007 (2009).
[10] Y. Kawamura, H. Yamamoto, K. Goushi, H. Sasabe, C. Adachi, and H. Yoshizaki, Appl. Phys. Lett. **84**, 2724 (2004).
[11] Y. Kawamura, H. Sasabe, and C. Adachi, Jpn. J. Appl. Phys., Part 1 **43**, 7729 (2004).
[12] R. R. Lunt, N. C. Giebink, A. A. Belak, J. B. Benziger, and S. R. Forrest, J. Appl. Phys. **105**, 053711 (2009).
[13] E. B. Namdas, A. Ruseckas, I. D. W. Samuel, S. C. Lo, and P. L. Burn, Appl. Phys. Lett. **86**, 091104 (2005).
[14] N. C. Giebink, Y. Sun, and S. R. Forrest, Org. Electron.: Phys., Mater., Appl. **7**, 375 (2006).
[15] T. Tsuboi and N. Aljaroudi, Opt. Mater. **30**, 1375 (2008).
[16] T. Kobayashi, N. Ide, N. Matsusue, and H. Naito, Jpn. J. Appl. Phys., Part 1 **44**, 1966 (2005).
[17] Y. Kawamura, J. Brooks, J. J. Brown, H. Sasabe, and C. Adachi, Phys. Rev. Lett. **96**, 017404 (2006).
[18] J. C. Ribierre, A. Ruseckas, K. Knights, S. V. Staton, N. Cumpstey, P. L. Burn, and I. D. W. Samuel, Phys. Rev. Lett. **100**, 017402 (2008).
[19] C. Tonnelé, M. Stroet, B. Caron, A. J. Clulow, R. C. R. Nagiri, A. K. Malde, P. L. Burn, I. R. Gentle, A. E. Mark, and B. J. Powell, Angew. Chem., Int. Ed. **56**, 8402 (2017).
[20] S. Sanderson, B. Philippa, G. Vamvounis, P. L. Burn, and R. D. White, J. Chem. Phys. **150**, 094110 (2019).
[21] L. Zhang, H. van Eersel, P. A. Bobbert, and R. Coehoorn, Chem. Phys. Lett. **652**, 142 (2016).
[22] S. Sanderson, B. Philippa, G. Vamvounis, P. L. Burn, and R. D. White, Appl. Phys. Lett. **115**, 263301 (2019).
[23] V. Jankus, C. Winscom, and A. P. Monkman, J. Chem. Phys. **130**, 074501 (2009).
[24] Y. Q. Zhang, G. Y. Zhong, and X. A. Cao, J. Appl. Phys. **108**, 083107 (2010).
[25] H. Kuhn, J. Chem. Phys. **53**, 101 (1970).
[26] Y. Kawamura, K. Goushi, J. Brooks, J. J. Brown, H. Sasabe, and C. Adachi, Appl. Phys. Lett. **86**, 071104 (2005).
[27] T. Lee, B. Caron, M. Stroet, D. M. Huang, P. L. Burn, and A. E. Mark, Nano Lett. **17**, 6464 (2017).

[28]M. Gao, T. Lee, P. L. Burn, A. E. Mark, A. Pivrikas, and P. E. Shaw, Adv. Funct. Mater. **30**, 1907942 (2019).
[29]X. Ren, J. Li, R. J. Holmes, P. I. Djurovich, S. R. Forrest, and M. E. Thompson, Chem. Mater. **16**, 4743 (2004).
[30]A. Endo and C. Adachi, Chem. Phys. Lett. **483**, 224 (2009).
[31]C. Adachi, R. C. Kwong, P. Djurovich, V. Adamovich, M. A. Baldo, M. E. Thompson, and S. R. Forrest, Appl. Phys. Lett. **79**, 2082 (2001).
[32]A. R. G. Smith, P. L. Burn, and B. J. Powell, ChemPhysChem **12**, 2429 (2011).
[33]M. E. O'Neill, "PCG: A family of simple fast space-efficient statistically good algorithms for random number generation," Technical Report No. HMC-CS-2014-0905, Harvey Mudd College, Claremont, CA, 2014.
[34]E. J. W. List, U. Scherf, K. Müllen, W. Graupner, C.-H. Kim, and J. Shinar, Phys. Rev. B **66**, 235203 (2002).
[35]S. M. King, D. Dai, C. Rothe, and A. P. Monkman, Phys. Rev. B **76**, 085204 (2007).
[36]J. C. Ribierre, A. Ruseckas, I. D. W. Samuel, S. V. Staton, and P. L. Burn, Phys. Rev. B **77**, 085211 (2008).
[37]D. L. Dexter, J. Chem. Phys. **21**, 836 (1953).
[38]W. Zhou, C. Zimmermann, and C. Jungemann, J. Appl. Phys. **125**, 165501 (2019).
[39]U. Neupane, B. Bahrami, M. Biesecker, M. F. Baroughi, and Q. Qiao, Nano Energy **35**, 128 (2017).
[40]R. Coehoorn, H. van Eersel, P. Bobbert, and R. Janssen, Adv. Funct. Mater. **25**, 2024 (2015).
[41]T. Förster, Ann. Phys. **437**, 55 (1948).
[42]C. Groves, Rep. Prog. Phys. **80**, 026502 (2017).
[43]M. C. Heiber and A. Dhinojwala, J. Chem. Phys. **137**, 014903 (2012).
[44]M. Scheidler, U. Lemmer, R. Kersting, S. Karg, W. Riess, B. Cleve, R. F. Mahrt, H. Kurz, H. Bässler, E. O. Göbel, and P. Thomas, Phys. Rev. B **54**, 5536 (1996).
[45]R. Richert and H. Bässler, J. Chem. Phys. **84**, 3567 (1986).
[46]N. Schmid, A. P. Eichenberger, A. Choutko, S. Riniker, M. Winger, A. E. Mark, and W. F. van Gunsteren, Eur. Biophys. J. **40**, 843 (2011).
[47]A. K. Malde, L. Zuo, M. Breeze, M. Stroet, D. Poger, P. C. Nair, C. Oostenbrink, and A. E. Mark, J. Chem. Theory Comput. **7**, 4026 (2011).
[48]M. J. Abraham, T. Murtola, R. Schulz, S. Páll, J. C. Smith, B. Hess, and E. Lindahl, SoftwareX **1-2**, 19 (2015).
[49]H. J. C. Berendsen, J. P. M. Postma, W. F. van Gunsteren, A. Dinola, and J. R. Haak, J. Chem. Phys. **81**, 3684 (1984).
[50]I. G. Tironi, R. Sperb, P. E. Smith, and W. F. van Gunsteren, J. Chem. Phys. **102**, 5451 (1995).
[51]B. Hess, H. Bekker, H. J. C. Berendsen, and J. G. E. M. Fraaije, J. Comput. Chem. **18**, 1463 (1997).